graphs, according to the only available data on networks, A is proportional to the segmental orientation function. Detailed calculations of the segmental orientation function in networks has been given recently.[12]

Acknowledgment. This work was supported by NATO Grant No. 85-0367.

References and Notes

(1) Viovy, J. L.; Monnerie, L.; Brochon, J. C. *Macromolecules* **1983**, *16*, 1845.
(2) Viovy, J. L.; Monnerie, L.; Merola, F. *Macromolecules* **1985**, *18*, 1130.
(3) Viovy, J. L.; Monnerie, L. *Polymer* **1986**, *27*, 181.
(4) Viovy, J. L. Thèse Doctorat ès-Sciences, Paris, 1983.
(5) Viovy, J. L.; Frank, C. W.; Monnerie, L. *Macromolecules* **1985**, *18*, 2607.
(6) Monnerie, L. *Static and Dynamic Properties of the Polymeric Solid State*; Pethrick, R. A., Richards, R. W., Eds.; D. Reidel: Dordrecht, 1982; p 383.
(7) Jasse, B.; Koenig, J. L. *J. Polym. Sci., Polym. Phys. Ed.* **1979**, *17*, 799.
(8) Amram, B.; Bokobza, L.; Queslel, J. P.; Monnerie, L. *Polymer* **1986**, *27*, 877.
(9) Flory, P. J. *J. Chem. Phys.* **1977**, *66*, 5720.
(10) Valeur, B.; Jarry, J. P.; Gény, F.; Monnerie, L. *J. Polym. Sci., Polym. Phys. Ed.* **1975**, *13*, 667, 675.
(11) Helfand, E. H. *J. Chem. Phys.* **1971**, *54*, 4651.
(12) Erman, B.; Monnerie, L. *Macromolecules* **1985**, *18*, 1985.
(13) Queslel, J. P.; Erman, B.; Monnerie, L. *Macromolecules* **1985**, *18*, 1991.
(14) Erman, B.; Flory, P. J. *Macromolecules* **1983**, *16*, 1601.
(15) Erman, B.; Flory, P. J. *Macromolecules* **1983**, *16*, 1607.
(16) Erman, B. *B. Polym. J.* **1985**, *17*, 140.
(17) Jarry, J. P.; Erman, B.; Monnerie, L. *Macromolecules*, following paper in this issue.
(18) Jarry, J. P.; Monnerie, L. *J. Polym. Sci., Polym. Phys. Ed.* **1978**, *16*, 443.
(19) Valeur, B.; Jarry, J. P.; Gény, F.; Monnerie, L. *J. Polym. Sci., Polym. Phys. Ed.* **1975**, *13*, 675.
(20) Jarry, J. P.; Monnerie, L. *Macromolecules* **1979**, *12*, 927.
(21) Abe, Y.; Flory, P. J. *J. Chem. Phys.* **1970**, *52*, 2814.

Segmental Mobility in Deformed Amorphous Polymeric Networks. 2. Experimental Study of Polyisoprene Using the Fluorescence Polarization Technique

J. P. Jarry,† B. Erman,‡ and L. Monnerie*

Laboratoire de Physicochimie Structurale et Macromoléculaire, associé au C.N.R.S., E.S.P.C.I., 10 rue Vauquelin, 75231 Paris Cedex 05, France. *Received April 30, 1986*

ABSTRACT: Results of measurements of segmental mobility by the fluorescence polarization technique are reported for 1,4-*cis*-polyisoprene networks under uniaxial tension at various temperatures and swelling ratios. Experimental data for the mean orientational mobility and anisotropy of mobility resulting from deformation are compared with predictions of the general theory given in the preceding paper.

Introduction

The steady-state dynamics of chains in a deformed network are affected by swelling, temperature, and the state of macroscopic strain. Changes in the dynamics upon deformation depend also on the constitution of the network, determined by factors such as configurational properties of chains and density of cross-linking. Macroscopic distortion of the network, as in the uniaxial stretching experiment, for example, changes the dimensions of chains and of the surrounding domains of local entanglements. The resulting change in configurations of chains and in the strength of local constraints modifies the dynamics to an experimentally measurable extent. In the present paper, results of fluorescence polarization measurements of segmental mobility on deformed polyisoprene networks at equilibrium are reported and compared with theoretical predictions of the preceding paper[1] (called I hereafter).

The fluorescence polarization technique is a convenient method of measuring the orientation and mobility of fluorescent labels attached to specific locations on a small number of chains of the network. The basic principle of the technique rests on the measurement of orientations of labels at two different times, from which the segmental orientation, mean segmental mobility, and dependence of mobility of segments on direction of stretch may be deduced.[2,3]

Fluorescence Polarization Technique

Fluorescence polarization has been used either to study mobility in isotropic systems or to measure the molecular orientation in frozen systems. The theory of this technique has been extended to the case of a uniaxial distribution of molecules[3] and hereafter we briefly review the main conclusions.

The absorption (or emission) properties of a fluorescent molecule can be described through the absorption (or emission) transition moment, $\mathbf{M}_a$ (or $\mathbf{M}_e$). Another characteristic is the mean lifetime, τ, of the excited state of the fluorescent molecule, commonly called the fluorescent lifetime. The most frequent values of τ range from 10^{-9} to 10^{-7} s.

Let us first assume that the transition moments $\mathbf{M}_a$ and $\mathbf{M}_e$ coincide with a molecular axis $\mathbf{M}$ of the fluorophore and that the polarization of the exciting radiation and fluorescence is not affected by the birefringence of the anisotropic sample. The effects arising from delocalization of the transition moments and from birefringence will be dealt with subsequently.

The direction of the unit vector $\mathbf{M}$ is specified by the spherical polar angles $\Omega = (\alpha,\beta)$ with respect to a reference frame $O(x,y,z)$ fixed to the sample, as shown in Figure 1. $N(\Omega_0,t_0)$ is the angular distribution function of $\mathbf{M}$ at time t_0 ($\mathbf{M}_0$ in Figure 1). $P(\Omega,t;\Omega_0,t_0)$ is the conditional probability density of finding at position Ω at time t a vector $\mathbf{M}$

† Permanent address: Rhône-Poulenc Films, Usine St-Maurice de Beynost, 01700 Miribel, France.
‡ Permanent address: School of Engineering, Bogazici University, Bebek, Istanbul, Turkey.

0024-9297/86/2219-2750$01.50/0

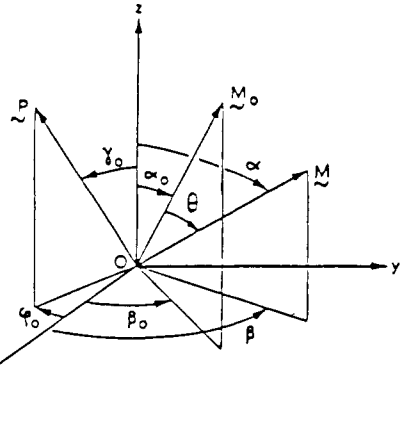

Figure 1. Positions of the molecular axis at t_0 and t indicated by the vectors $\mathbf{M}_0$ and $\mathbf{M}$, respectively. The system $Oxyz$ denotes the laboratory-fixed coordinate system. Spherical angles (α_0,β_0) and (α,β) specify the orientational configurations of $\mathbf{M}_0$ and $\mathbf{M}$, respectively. Spherical angles (γ_0,φ_0) define the position of the polarizer $\mathbf{P}$.

that was at position Ω_0 at time t_0. After the sample is illuminated by a linearly polarized short pulse of light at t_0, the intensity emitted at time $(t_0 + u)$ for the $\mathbf{P}$ and $\mathbf{A}$ directions of polarizer and analyzer is given by

$$i(\mathbf{P},\mathbf{A},t_0,u) = K\int\int N(\Omega_0,t_0)P(\Omega,t;\Omega_0,t_0) \times \cos(\mathbf{P},\mathbf{M}_0)\cos(\mathbf{A},\mathbf{M})\exp(-u/\tau)\,d\Omega_0\,d\Omega \quad (1)$$

where K is an instrumental constant. In this expression t_0 corresponds to a macroscopic evolution of the sample whereas u corresponds to a microscopic reorientational motion on the scale of the fluorescence lifetime τ. In most cases the t_0 dependence of N and P can be ignored within the time τ, and the fluorescence intensity emitted under continuous excitation is given by

$$i(\mathbf{P},\mathbf{A},t_0,\tau) = \int_0^\infty i(\mathbf{P},\mathbf{A},t_0+u)\,du \quad (2)$$

An expansion of the angular functions of Ω_0 and Ω in a series of spherical harmonics $Y_l^m(\Omega_0)$ and $Y_l^m(\Omega)$ leads to the following expressions:

$$\cos^2(\mathbf{P},\mathbf{M}_0) = \sum_{k=0}^{\infty}\sum_{m=-k}^{k} p_k^m(\gamma_0,\varphi_0)Y_k^m(\Omega_0)$$

$$\cos^2(\mathbf{A},\mathbf{M}) = \sum_{k=0}^{\infty}\sum_{m=-k}^{k} a_k^m(\gamma,\varphi)Y_k^m(\Omega)$$

$$i(\mathbf{P},\mathbf{A},t_0,\tau) = \sum_{k=0}^{\infty}\sum_{l=0}^{\infty}\sum_{m=-k}^{k}\sum_{n=-l}^{l} p_k^m a_l^n f_{kl}^{mn}(t_0,\tau) \quad (3)$$

with

$$f_{kl}^{mn}(t_0,\tau) = K\int_0^\infty \langle \bar{Y}_k^m(\Omega_0)Y_l^n(\Omega)\rangle \exp(-u/\tau)\,du \quad (4)$$

where p_k^m and a_k^m characterize the positions of $\mathbf{P}$ and $\mathbf{A}$, the overbar denotes the complex conjugate, and the angular brackets mean an ensemble average.

For the case of uniaxial symmetry about the Oz axis, only the first six nonzero terms f_{kl}^{mn} are sufficient to characterize the orientation and the mobility of the system:

$$f_{00}^0,\ f_{20}^0,\ f_{02}^0,\ f_{22}^0,\ f_{22}^1,\ f_{22}^2 \quad (5)$$

where f_{00}^0 is simply

$$f_{00}^0 = K/4\pi \quad (6)$$

More convenient quantities can be defined from the remaining f terms

$$G_{20}^0 = (1/5)^{1/2}(f_{20}^0/f_{00}^0) = (1/2)\langle 3\cos^2\alpha_0 - 1\rangle$$

$$G_{02}^0 = (1/5)^{1/2}(f_{02}^0/f_{00}^0) = (1/2)\langle 3\cos^2\alpha - 1\rangle$$

$$G_{22}^0 = (1/5)(f_{22}^0/f_{00}^0) = (1/4)\int_0^\infty \langle(3\cos^2\alpha_0 - 1)(3\cos^2\alpha - 1)\rangle \exp(-u/\tau)\,du$$

$$G_{22}^1 = (3/40)(f_{22}^1/f_{00}^0) = (9/16)\int_0^\infty \langle\sin\alpha_0\cos\alpha_0\sin\alpha\cos\alpha\cos(\beta-\beta_0)\rangle \exp(-u/\tau)\,du$$

$$G_{22}^2 = (3/40)(f_{22}^2/f_{22}^0) = (9/64)\int_0^\infty \langle\sin^2\alpha_0\sin^2\alpha\cos^2(\beta-\beta_0)\rangle \exp(-u/\tau)\,du \quad (7)$$

This set of equations is analogous to eq I-8 for the case of fluorescence polarization under continuous illumination.

The quantities G_{20}^0 and G_{02}^0 represent the molecular orientation of the sample at time t_0 and $(t_0 + u)$ and are independent of molecular mobility. Under the assumption of equilibrium, the molecular orientation distribution is invariant, and $G_{20}^0 = G_{02}^0$. It should be noted that this equality is still valid, as a first approximation, for systems that are out of equilibrium, provided that the molecular orientation distribution does not change significantly on the time scale of the fluorescent lifetime, which is ca. 10^{-8} s.

The three other quantities G_{22}^m depend on both the molecular orientation and the mobility. However, new functions dealing with only the mobility of the fluorescent molecules in different directions can be defined as

$$M(\tau) = \int_0^\infty \langle(3\cos^2\theta(u) - 1)/2\rangle \exp(-u/\tau)\,du$$

$$M(\tau) = G_{22}^0 + (16/3)G_{22}^1 + (16/3)G_{22}^2$$

$$4D - S = 2G_{20}^0 - 2G_{22}^0 - (16/3)G_{22}^1 + (32/3)G_{22}^2$$

$$3D - C = G_{20}^0 - 2G_{22}^0 - (16/3)G_{22}^1 + (32/3)G_{22}^2$$

$$A = (1/3)[G_{20}^0 + (3D - C)] \quad (8)$$

Definitions of functions M, C, D, and S are given in eq I-10. C deals with the orientation–mobility correlation, D reflects the directivity of mobility, S reflects the sense of mobility, and A is related to the anisotropy of mobility. $M(\tau)$ is an inverse measure of the mean segmental mobility, and in the sequel we will use a more convenient quantity, the mobility parameter, m:

$$m = M^{-1}(\tau) - 1 \quad (9)$$

which increases from zero (molecular relaxation times much larger than the fluorescence lifetime) to infinity (relaxation times much smaller than the lifetime).

In many fluorescent molecules, the transition moments in absorption and emission do not coincide. In isotropic systems, this delocalization effect is usually described in terms of the limiting emission anisotropy r_0. When delocalization occurs in uniaxially oriented systems, it is quite easy to correct for this effect[3] with an additional measurement of r_0 in the isotropic state.[4]

The birefringence effect occurs when the direction of the polarizer $\mathbf{P}$ and of the analyzer $\mathbf{A}$ does not coincide with a principal direction of the refractive index tensor. Only the G_{22}^1 autocorrelation function is affected by birefringence, and a correction factor b_0 must be determined from independent birefringence measurements performed on the polymer under study.[3,5]

Thus, in the case of a system where delocalization occurs and birefringence has to be considered, measurement of

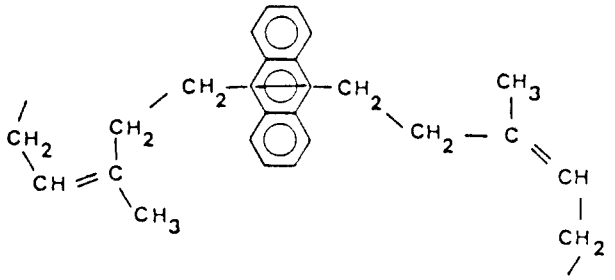

Figure 2. Portion of the polyisoprene chain with the anthracene unit as the label. The double arrow indicates the direction of the transition moment.

fluorescence intensities for different directions of polarizer and analyzer leads to quantities γ^m_{kl}, which are related to the quantities G^m_{kl} by the equations

$$\gamma^0_{20} = (5r_0/2)^{1/2}G^0_{20}$$
$$\gamma^0_{22} = (5r_0/2)G^0_{22}$$
$$\gamma^1_{22} = (5r_0/2)b_0G^1_{22}$$
$$\gamma^2_{22} = (5r_0/2)G^2_{22} \quad (10)$$

In order to get all the intensity measurements required to derive the γ^m_{kl} quantities, specific equipment has been designed[5] and used in the present study. The purpose of the apparatus is to measure simultaneously a convenient set of intensities $i(\mathbf{P},\mathbf{A})$ yielding at least five independent equations. This is achieved in using two orientations of **P** and three orientations of **A** that are not contained in the same plane. The details on the equipment as well as the method of derivation of the γ^m_{kl} quantities from the various measured intensities are reported elsewhere.[3,5]

Material

The polymer investigated was an anionic polyisoprene (Shell IR 307) of high molecular weight ($M_n \simeq 500\,000$) with high cis-1,4 configuration (92%). It was carefully purified by extraction with ethanol. Labeled anionic polyisoprene chains were prepared by using a method analogous to that reported previously for polystyrene.[5] Monofunctional "living" chains of molecular weight 300 000 were synthesized and deactivated by 9,10-bis(bromomethyl)anthracene. Each of the resulting chains of molecular weight 600 000 contains an anthracene fluorescent group at its center, as shown in Figure 2. The advantage of this method of labeling is that the transition moment of the anthracene group, the orientation and the mobility of which are measured, lies along the local chain axis. In particular, it cannot undergo any motion independently of the chain backbone. Furthermore, it has to be pointed out that the fluorescence polarization does not provide an absolute determination of the second moment of the orientation distribution, G^0_{20}, of the chain statistical segments. The measured quantity is the orientation function $G^0_{20}(\mathbf{M})$ of the transition moment of the fluorescent label, which is proportional to G^0_{20}:

$$G^0_{20}(\mathbf{M}) = fG^0_{20} \quad (11)$$

An interesting feature of the type of labeling used in this study is that the collinearity of the transition moment and the local chain axis leads to a positive value of the coefficient f.

The labeled polymer (1% by weight) and purified IR 307 polyisoprene (99%) were mixed in solution, and the solvent was removed by evaporation. Samples were molded and cross-linked with dicumyl peroxide at 147 °C for 40 min. The amounts of dicumyl peroxide used were 0.5, 1, and 2% by weight for samples I, II, and III, respectively. The cross-linking density was characterized by the mean molecular weight M_c of network chains (between adjacent network junctions) derived from measurements of the equilirium swelling ratio. Three cross-linking densities have been studied: sample I, $M_c = 1.1 \times 10^4$; sample II, $M_c = 2 \times 10^4$; sample III, $M_c = 4 \times 10^4$.

Determination of mobility characteristics requires the use of the autocorrelation function G^1_{22}, the measurement of which is affected by the birefringence of the stretched sample. In order to obtain G^1_{22} with a satisfactory accuracy when high values of birefringence are reached during the stretching, it is necessary to use samples with a thickness of 0.2 mm.

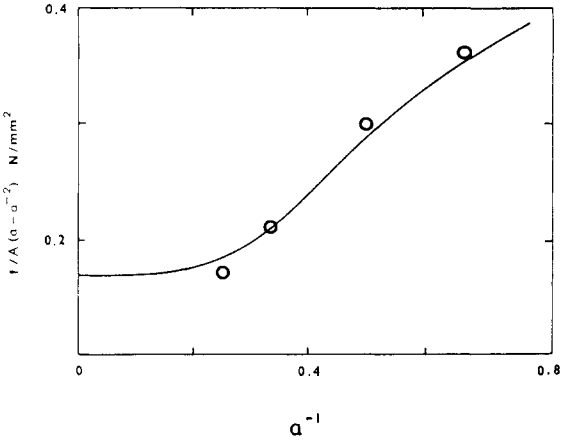

Figure 3. Relationship of reduced stress to reciprocal extension ratio, α^{-1}, for sample II. The reduced stress is defined as $f/A(\alpha - \alpha^{-2})$, where f is force and A is the cross-sectional area. Circles represent experimental data, and the curve is from theory, with $\xi kT/V_0 = 0.19$ N/mm^2, $\kappa = 9$, and $\zeta = 0.025$. (See ref 8 and 9 for details of calculations.)

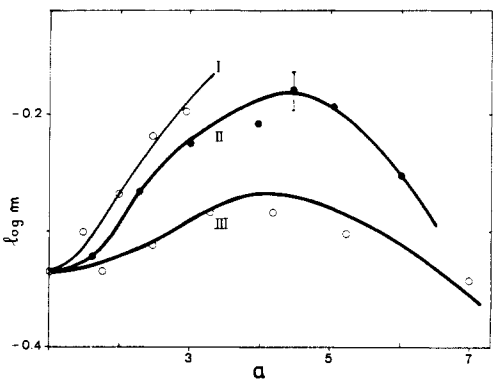

Figure 4. Effect of cross-linking density on mobility, m, presented as a function of deformation ratio, α. Points show results of experiments for three different samples. Curves are obtained according to the theory. Error bar shown on one of the data points is representative for all data points. Results are for dry network at 25 °C.

Results of Experiments

Measurements of mobility on undeformed polyisoprene networks at various temperatures and swelling ratios were previously published.[7] The present study deals with the strain dependence data which were presented in J. P. Jarry's thesis.[2]

Results of measurements are shown by the circles in Figures 3–8. The curves through the experimental points are obtained by theoretical calculations to be explained in the following section.

The mobility data are represented by the logarithmic scale along the ordinate for mobility for the purpose of convenience only.

Effect of Cross-Linking. The logarithm of mean mobility, m, for the three networks at 25 °C is shown as a function of extension ratio, α, in Figure 4. α is the ratio of final length to initial undistorted length of the samples.

The data points show the pronounced effect of the degree of cross-linking on the strain dependence of mobility.

The experiment on the high cross-link density sample I was terminated at about $\alpha = 3$ due to rupture. Samples II and III exhibit maxima for mobility at $\alpha \simeq 4.5$ and 4,

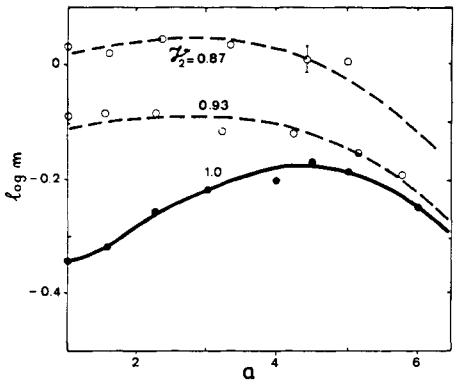

Figure 5. Effect of swelling on mobility presented as a function of deformation. Points show results of experiments for sample II at 25 °C. Curves are calculated according to theory.

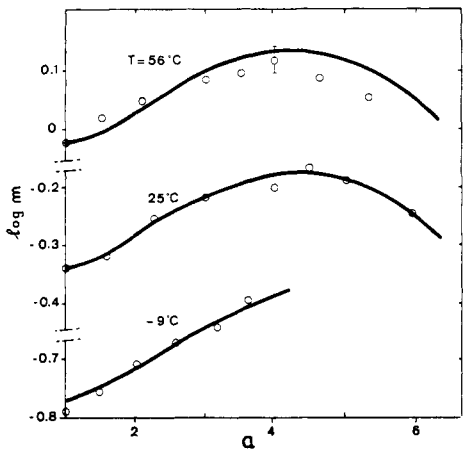

Figure 6. Effect of temperature on mobility for sample II presented as a function of deformation. See legend to Figure 4.

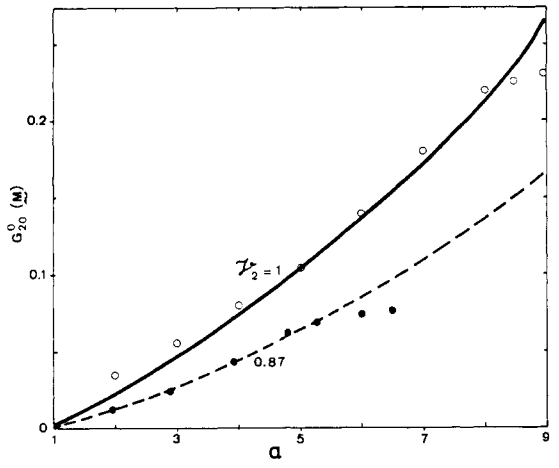

Figure 7. Orientation function of the transition moment of the label presented as a function of deformation. Points represent experimental results for dry (empty circles) and swollen (filled circles) samples. Curves are calculated from theory.

respectively. Mobility values for the three networks extrapolate to a common intercept at $\alpha = 1$, indicating that local chain dynamics of undeformed samples is unperturbed by cross-linking.

Effect of Swelling. Results of mean mobility for the dry network (sample II) are compared with those for two degrees of swelling in Figure 5. The swelling agent was toluene and the measurements were performed at 25 °C. Experimental data show that the pronounced maximum for m for the dry network disappears upon swelling. Although the degree of swelling is not much ($\nu_2 = 0.87$ and

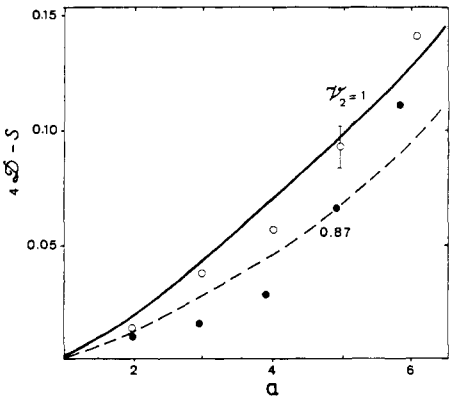

Figure 8. Dependence of directivity of mobility, D, on deformation. Points represent experimental results for dry (empty circles) and swollen (filled circles) samples. Curves show the orientation curves of Figure 7.

0.93), its effect on the strain dependence of mobility is abrupt as indicated by the three sets of experimental points in Figure 5. The $\alpha = 1$ intercepts correspond to mobility in the undistorted network. The three data points at this intercept show that m is approximately linear in ν_2 in the interval $0.87 < \nu_2 < 1$ (see also ref 7).

Effect of Temperature. The strain dependence of mobility at three different temperatures is shown by the three sets of experimental data points in Figure 6 for sample II. Results show that changing the temperature does not affect the form of the strain dependence of mobility but only shifts the $\alpha = 1$ intercept. Values of mobility at different temperatures in undeformed networks are in close agreement with the WLF hypothesis.[7]

Relationship between Orientation and Anisotropy of Mobility. Values of the orientation function, G^0_{20}, are shown as a function of α by the two sets of data points in Figure 7. Empty and filled circles represent results for sample II for $\nu_2 = 1$ and 0.87, respectively. The corresponding data for the function $4D - S$ (given by I.10 and I.11) are presented in Figure 8. Comparison of Figures 7 and 8 shows that, within experimental accuracy, $4D - S = G^0_{20}$, for both the dry and the swollen network throughout the full range of α covered.

Comparison of Experiment with Theory and Discussion

According to the theory developed in I, the mobility, m, is expressed as a function of macroscopic strain, α, and the polymer fraction, ν_2. In order to reduce cross-reference, we write eq I.20 below in terms of α and ν_2, in a form ready for use in calculations for a tetrafunctional network. Accordingly

$$m = a(T,\nu_2)[1 + b\ \mathrm{tr}\ (\Lambda^2 - \Lambda_0^2) + c\ \mathrm{tr}\ (\Theta^2 - \Theta_0^2)] \quad (12)$$

with

$$\mathrm{tr}\ (\Lambda^2 - \Lambda_0^2) = (\nu_2^{-2/3}/2)(\alpha^2 + 2\alpha^{-1} - 3) + [B(\alpha) + 2B(\alpha^{-1/2}) - 3B(1)]/2$$

$$\mathrm{tr}\ (\Theta^2 - \Theta_0^2) = g(\alpha)B(\alpha) + 2g(\alpha^{-1/2})B(\alpha^{-1/2}) - 3g(1)B(1) \quad (13)$$

where

$$B(\alpha) = \frac{(\alpha\nu_2^{-1/3} - 1)(\alpha\nu_2^{-1/3} + 1 - \zeta\alpha^2\nu_2^{-2/3})}{[1 + g(\alpha)]^2} \quad (14)$$

$$g(\alpha) = \nu_2^{-2/3}\alpha^2[\kappa^{-1} + \zeta(\nu_2^{-1/3}\alpha - 1)]$$

tr denotes the trace operator, and the coefficients b and c in eq 12 acknowledge proportionality of mobility to the

first invariants tr $(\Lambda^2 - \Lambda_0^2)$ and tr $(\Theta^2 - \Theta_0^2)$ of the molecular deformation tensor and the domain constraint tensor, respectively. Values of the functions $B(\alpha^{-1/2})$, $B(1)$, $g(\alpha^{-1/2})$, and $g(1)$ appearing in eq 13 may be obtained from the corresponding expressions in eq 14 by replacing α by $\alpha^{-1/2}$ and 1. The material parameters κ and ζ (defined in I) represent deviations from the phantom network theory. For $\kappa = 0$, the function B vanishes and m becomes proportional to the first invariant of the macroscopic deformation tensor α. For a given network, values of κ and ζ may conveniently be obtained from the stress–strain data. For sample II, the best fit to stress–strain data, shown in Figure 3, was obtained by choosing $\kappa = 9$ and $\zeta = 0.025$. The expression for the stress according to the molecular model is given elsewhere.[8] For samples I and III, experimental stress–strain data were not available. κ is chosen as 6.7 for sample I and 12.7 for sample III, in inverse proportion to the square root of their cross-link densities (see ref 8 and the references cited therein for further discussion). ζ is taken as 0.025 for both.

The front factor $a(T,v_2)$ in eq 12 represents mobility in an undistorted network. Its dependence on polymer concentration in the swollen network and to temperature has been reported previously.[7] According to measurements, mobility in network at 25 °C swollen with toluene was approximately linear for $0.85 < v_2 < 1$. The temperature dependence of mobility, on the other hand, was in agreement with the WLF hypothesis at temperatures sufficiently above the glass transition temperature.[7]

The coefficient b in eq 12 reflects the effect of rotational isomerization upon stretching on chain mobility. Theory[1] suggests that it should vary inversely with chain length between cross-links. Inasmuch as b is associated with the intramolecular compliance to the rotational isomerization of the single chain, it should be independent of v_2. The coefficient c, on the other hand, simultaneously reflects the compliance to isomerization of portions of the chains in the entanglement domains and also the variation of the effects of constraints by deformation. The latter effect is a consequence of the coupling of segments to their environments through the elastic action of entanglements. In this respect, c is expected to be strongly dependent on v_2. The dependence of c on the length of network chains cannot be deduced from theoretical consideration. Its value should diminish, however, with increasing chain length in recognition of the effect of isomerization due to the local strain field surrounding the sequences of segments.

Inasmuch as the dependence of mobility on temperature is accounted for by the front factor a, the coefficients b and c are expected to be independent of temperature in first approximation.

Values of b and c leading to the best fit to experimental values of mobility shown in Figures 4–6 and satisfying the conditions stated in the above paragraphs are chosen by trial for sample II in the dry state as $b = -0.0283$ and $c = 0.239$. For the swollen state, reducing c to 0.08 while leaving b the same as above led to agreement with data. For samples I and III, values of b were −0.0515 and −0.0142, respectively, showing inverse relation to network chain length. Values of c for samples I and III for best fit to data are, respectively, 0.35 and 0.09. These values also show inverse relation to chain length. Values of all the parameters used in calculations for the three samples are summarized in Table I.

Results of calculations of mobility based on the above parameters and eq 12 are shown in Figures 4–6. Agreement with experimental data over wide ranges of strain and temperature for the dry and swollen networks is satisfactory. The negative value of b indicates that isomerization of the polyisoprene chain upon stretching slows down the mean orientational mobility of segments. This effect is much smaller, however, than that introduced by the local constraints. Calculations show that in the dry network, the contribution of the b term to mobility is only a few pecent for $\alpha < 3$. At large deformations ($\alpha = 6$) or in the swollen state, the contribution of the b term on mobility becomes significant, however.

Table I

sample	$M_c \times 10^{-4}$	κ	ζ	b	c	d	e
I	1.1	6.7	0.025	−0.0515	0.35		
					0.239	0.006	
II	2	9.0	0.025	−0.0283			1.4
					(0.08)[a]	(0.0035)[a]	
III	4	12.7	0.025	−0.0142	0.09		

[a] Values in parentheses are to be used for $v_2 = 0.93$ or 0.87.

The decrease in mobility observed at deformations exceeding 4 are not correlated with finite chain extension effects because the maximum for sample III is at a lower α value than that for sample II. Inasmuch as the chains in sample III are longer than those in sample II, possible correlation of the maxima with finite chain extension effects would dictate the appearance of the maximum for sample III at much higher strains than those observed in Figure 4. The Mooney–Rivlin plot of the reduced stress for sample II exhibits an upturn at values of α exceeding 6. For sample III, with chains twice as long as those of sample II, the upturn is expected to commence between $\alpha = 8$ and $\alpha = 9$.

In Figure 7, results of calculations of G_{20}^0 for sample II in the dry state (solid curve) and for $v_2 = 0.87$ (dashed curve) are shown. The circles represent experimental data. Equation I.19, when expressed in terms of α and v_2 for a tetrafunctional network, reads as

$$G_{20}^0 = (D/2)[v_2^{-2/3}(\alpha^2 - \alpha^{-1}) + B(\alpha) - B(\alpha^{-1/2}) + 2e\{g(\alpha)B(\alpha) - g(\alpha^{-1/2})B(\alpha^{-1/2})\}] \quad (15)$$

where the functions B and g are given by eq 14 and D and e are the material parameters defined previously. For the dry network, agreement with experiment requires $D = 0.006$ and $e = 1.4$. For the swollen network, D has to be decreased to 0.0035. Discussion of the mechanism affecting orientation and physical interpretation of the coefficients D and e are given elsewhere.[8,9]

Experimental measurements of the function $4D - S$, presented in Figure 8, show that this quantity is approximately equal to G_{20}^0. The curves in Figure 8 show the values of G_{20}^0 calculated from eq 15. It can be concluded, therefore, that within experimental accuracy

$$4D - S = G_{20}^0 \quad (16)$$

for this sample II. Also, from eq I.12, we have

$$D + C - S = G_{20}^0 \quad (16')$$

Subtracting eq 16′ from eq 16, we obtain

$$3D - C = 0 \quad (17)$$

Substituting eq 17 into eq I-18 shows that only static orientations contribute to A:

$$A = G_{20}^0/3 \quad (18)$$

The expression for A given by eq 18 is positive for all values of α and hence indicates that mobility of segments along the direction of stretch is more intense than that along the lateral direction.

It should be noted that the conclusions reached in the preceding paragraph, according to which anisotropy of mobility is dependent only on the static orientation function, are results of experimental observations for the polyisoprene network. The dynamic contributions to anisotropy of mobility may not be negligibly small for other polymer systems, in general. More conclusive discussion on this subject awaits further experimental work on different polymeric systems.

Conclusions

Comparison of the predictions of the theory with experimental data on mean mobility and anisotropy of mobility shows the following. (i) The mean segmental mobility in undeformed networks increases linearly with swelling in the range $v_2 > 0.85$ and according to the WLF law with temperature. (ii) The mean segmental mobility is proportional to the combination of first invariants of the molecular deformation tensor and the deformation tensor of constraint domains. Proportionality to the former reflects effects of rotational isomerization of a stretched chain on the mobility of its segments, whereas proportionality to the latter reflects effects of coupling of sequences of segments to their surroundings. Increase of mobility up to $\alpha = 4$ is indicative of the dilation of constraint domains upon stretching. Decrease of mobility for strains exceeding $\alpha = 4$ reflects the effect of increase of local constraints at high strains. On the other hand, isomerization of the stretched polyisoprene chain results in a decrease of mean segmental mobility at all levels of strain. (iii) Swelling of the network drastically decreases the effect of the constraints on segmental mobility, whereas the effect of isomerization is independent of swelling. (iv) The strain dependence of mean segmental mobility is not affected by temperature. (v) To the first-order approximation, within experimental accuracy, the anisotropy of mobility is proportional to the orientation function. It may be concluded that mobility of segments along the direction of stretch for the polyisoprene network is larger than those along lateral directions.

Acknowledgment. This work was supported by NATO Grant No. 85-0367. We are grateful for the samples received from Manufacture Française des Pneumatiques Michelin (Clermont-Ferrand, France).

References and Notes

(1) Erman, B.; Monnerie, L. *Macromolecules*, previous paper in this issue.
(2) Jarry, J. P. Thèse Doctorat ès-Sciences, Paris, 1978.
(3) Jarry, J. P.; Monnerie, L. *J. Polym. Sci., Polym. Phys. Ed.* **1978**, *16*, 443.
(4) Jablonski, A. *Z. Naturforsch., A: Astrophys., Phys. Phys. Chem.* **1961**, *16a*, 1.
(5) Jarry, J. P.; Pambrun, C.; Sergot, Ph.; Monnerie, L. *J. Phys. E* **1978**, *11*, 702.
(6) Valeur, B.; Monnerie, L. *J. Polym. Sci., Polym. Phys. Ed.* **1976**, *14*, 11.
(7) Jarry, J. P.; Monnerie, L. *Macromolecules* **1979**, *12*, 927.
(8) Erman, B.; Monnerie, L. *Macromolecules* **1985**, *18*, 1985.
(9) Queslel, J. P.; Erman, B.; Monnerie, L. *Macromolecules* **1985**, *18*, 1991.

Sol–Gel Transition and Phase Diagram of the System Atactic Polystyrene–Carbon Disulfide

Jeanne François, Joseph Y. S. Gan, and Jean-Michel Guenet*

Institut Charles Sadron (CRM-EAHP), CNRS/ULP, 67083 Strasbourg Cedex, France.
Received February 14, 1986

ABSTRACT: This paper deals with the determination of the phase diagram by means of calorimetry (DSC) of the physically gelling system atactic polystyrene (aPS)–carbon disulfide (CS_2). The investigation was carried out with different molecular weights. DSC results have been compared to those obtained by other techniques. The findings of Tan et al. are confirmed and particularly a gel formation exotherm is unmistakably shown as well as a broader gel melting endotherm. These thermal features are absent in solvents wherein physical gelation cannot take place. From the results, it is concluded that gelation in aPS–CS_2 solutions proceeds from a first-order transition that entails a mechanism of nucleation and growth. Accordingly, three-dimensional structures that possess a certain order are created. This is in total contradiction with the recent hypothesis of Boyer et al., who consider liquid-like contacts. In addition, both the phase diagram and the variation of either the formation or the melting enthalpies display a maximum near $C_{pol} \simeq 55\%$. After checking the absence of any artifact, we conclude that aPS and CS_2 form a polymer–solvent complex or a stoichiometric compound. This means that without solvent, physical links cannot be created, a statement in agreement with the fact that aPS cannot crystallize from the bulk.

Introduction

The occurrence of physical gelation of polymer solutions is generally thought to originate in chain crystallization and has been accordingly restricted to crystallizable polymers or at least stereoregular polymers. However, the propensity of *atactic polystyrene* (aPS) to form physical gels has been recently discovered by Tan et al.[1] and has received confirmation from rheological measurements.[2,3] In addition, the existence of aPS physical gelation has enabled Guenet et al. to provide a coherent explanation[4,5] for the so-called "enhanced low-angle scattering" (ELAS) observed in moderately concentrated solutions, which had been unaccounted for.

Once the principle of aPS physical gelation is accepted, the next step in gaining knowledge concerns the mechanism involved. If one considers that ELAS and gelation are simply different manifestations of the same phenomenon,[5] results gathered on semidilute solutions can be used to attempt to explain gelation. On this basis, Gan, François, and Guenet[5] recently suggested that ELAS is due

0024-9297/86/2219-2755$01.50/0